EVALUATION AND ANALYSIS OF COMPUTATIONS AND EXPERIMENTS FOR TRANSONIC WING BODY CONFIGURATIONS

G. Drougge, N. Agrell, S. Hedman, and L. Torngren
The Aeronautical Research Institute of Sweden (FFA)
S-161 11 Bromma, Sweden

ABSTRACT

At the 10th ICAS Congress in 1976 results were reported from the design of a wing-body combination. An inverse procedure based on the transonic small disturbance theory had been used.

The agreement between computed pressure distributions and measurements was encouraging and further analysis of the results, including evaluation of the wave-drag, revealed many features of great aerodynamic interest. This led to modifications in the use of the numerical method and in the wing-body design. The modified wing-body combination has again been tested and the results analyzed further. It is concluded that the inverse method can be a powerful design tool and that in any case for moderate aspect ratios the concept of a wing as formed from two-dimensional profiles can be replaced by the concept of a wing formed from two surfaces.

SYMBOLS

b	wing span
c	normalized local chord length
C_D	wing drag coefficient
C_L	wing lift coefficient
C_p	pressure coefficient
C_p^*	critical pressure coefficient
C_T	wing tangential force coefficient
c_n	wing section normal force coefficient
c_t	wing section tangential force coefficient
M_∞	Mach number in undisturbed stream
r	radius of body cylinder
R	fuselage radius
t	wing thickness
U_∞	free stream velocity
x,y,z	Cartesian coordinates
α	body angle of attack
γ	specific heat ratio
δ	average wing thickness ratio
ϵ	scaling factor
φ	perturbation velocity potential
ϕ	total velocity potential
η	$2y/b$ spanwise coordinate

INTRODUCTION

The relatively good agreement previously obtained[1] between experiments and calculations performed with the transonic small disturbance relaxation method was encouraging. It was therefore decided to evaluate the results further and also to do more wind tunnel tests and calculations. The earlier investigation on the so-called PT7 wing-body combination was restricted to comparing computed and measured chordwise pressure distributions at three sections and at a few transonic Mach numbers.

The present investigation includes calculation at a small lift coefficient of the pressure drag so that the drag curve and the critical Mach number can be compared with the corresponding results from wind tunnel balance tests. As will be shown later, the agreement is surprisingly good despite the fact that no viscous effects are taken into account in the calculation method.

In order to investigate the effects of a moderate change in wing geometry a new wing was designed which had smaller relative thickness at the inboard part of the wing. For this wing, designated PT9, only computations have been made. Due to cost and time limitations no actual wing could be constructed and tested. However, it turned out to be quite feasible to modify the PT7 body so that this new wing-body configuration, called PT7-9, obtained the same longitudinal distribution of cross sectional area as the PT9 wing with the original PT7 body. For the new configuration, PT7-9, both pressure distribution measurements and balance tests were performed.

The whole investigation can thus be summarized as an exercise in transonic wing-body design performed in order to gain confidence in the calculation method.

In this respect reference is also made to another paper[2] at this Congress.

METHOD OF CALCULATION

General

The basic method is described in reference 1 in detail. Only a summary is given here showing some modifications.

A perturbation potential φ is defined in terms of the full velocity potential ϕ,

$$\phi(x,y,z) = U_\infty[x + \epsilon\varphi(x,y,z)]$$

where the scaling factor ϵ is put $\epsilon = \delta^{2/3}/M_\infty$. δ is taken as the average wing thickness ratio. The transonic small disturbance equation is written in φ.

$$\left\{(1-M_\infty^2) - [3-(2-\gamma)M_\infty^2]M_\infty^2 \varepsilon\varphi_x\right\}\varphi_{xx}+\varphi_{yy}+\varphi_{zz}=0. \quad (1)$$

This equation is transformed into finite difference form and solved by the relaxation procedure introduced by Murman and Cole [3]. The mixed flow character is obtained through the use of centered differences in subsonic portions and upstream differences in supersonic portions of the field.

The surface of the configuration may be written as $z=f(x,y)$. For field points adjacent to the body the mass flux vector is required to be parallel to the configuration surface. The formulation of the corresponding boundary condition has been given [4]

$$\varphi_z=\left\{\frac{1}{\varepsilon}+(1-M_\infty^2)\varphi_x-\frac{1}{2}[3-(2-\gamma)M_\infty^2]M_\infty^2\varepsilon\varphi_x^2\right\}\frac{dz}{dx}+\varphi_y\frac{dz}{dy}$$

Far field expressions are used on the exterior of the computation domain. A consistent derivation of the pressure coefficient gives

$$C_p = \left\{-2\varepsilon\varphi_x-\varepsilon^2[(1-M_\infty^2)\varphi_x^2+\varphi_y^2+\varphi_z^2]+\right.$$
$$\left.+\varepsilon^3[3-(2-\gamma)M_\infty^2]M_\infty^2\,\varphi_x^3/3\right\}$$

The computer program can operate in two modes, direct and inverse. In the first it works as an analysis program and computes pressures for given geometry, and in the other it is a design program that produces surfaces for given pressures.

Lift and Drag Evaluation

The finite difference equation system used for the solution of (1) fully conserves the mass flow. However, the momentum is not conserved across shock waves, instead the momentum deficit is an estimate of the wave drag [5]. The drag is computed through an integration in the vertical direction of the pressure difference between points on the forward and the aft side of the airfoil respectively as shown in Figure 1.

$$C_T = \int_{\eta_{body}}^{1} \frac{c(\eta)}{\bar{c}} \int_{(z/c)_{min}}^{(z/c)_{max}} \Delta C_p\left(\frac{z}{c},\eta\right) d\left(\frac{z}{c}\right)\, d\eta$$

where C_T is the wing tangential force coefficient, η_{body} is the position of the wing body juncture, and

$$\bar{c} = \int_0^1 c(\eta)\, d\eta \,.$$

The upper loop in the Cp vs z/c plot gives a positive contribution to the section tangential force, while the lower loop gives a negative in the case shown. In reality the curve should have a vertical tangent at the stagnation point but neither the experiments nor the transonic small perturbation theory can give guidance to the local shape of the curve. Simple sweep considerations have given the leading edge value, and for the calculation of drag the pressure has been assumed to vary linearly between the data points. It will be shown later that this estimate permits a reasonable drag evaluation for the investigated Mach numbers.

The normal force is an integration of the pressure difference across the wing plan form. Normal and tangential forces are then transformed to lift and drag.

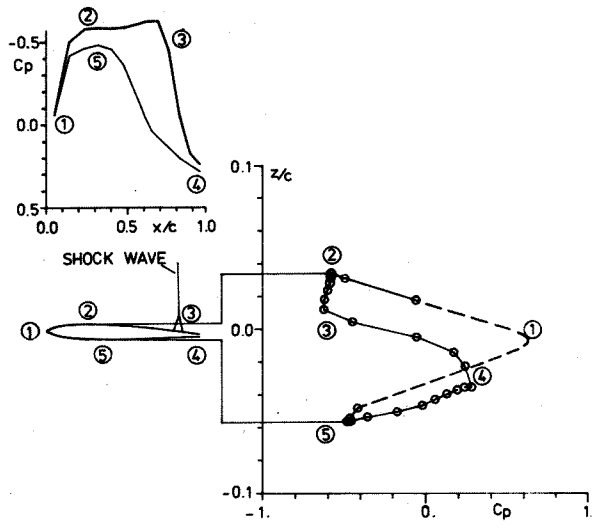

Figure 1 PRESSURES PLOTTED VERSUS x/c AND z/c RESPECTIVELY

Application

The calculation procedure described was used to compute pressure distributions and lift and drag coefficients for three configurations for some Mach numbers and angles of incidence. Boundary conditions were applied in the wing reference plane and on a cylindrical surface enscribing the body. The effect of the closed body noses was neglected and the bodies approximated by infinitely long cylinders. The contouring of the body in the wing body intersection region was included in accordance with slender body theory, i.e. the body slopes dR/dx were weighted with the ratio of body radius R to reference cylinder radius. The configurations were placed in a grid of field points with 41, 28, and 28 points in the x,y, and z directions respectively. The points were clustered in the vicinity of the wing as far as the method allowed. The first point on each wing section was situated in 5 % of the local chord. The extension of the computation domain can be seen in Figure 2. The scale is chosen so the wing root chord length becomes unity. Out of approximately 32000 points in total only 380 points define the two sides of starboard wing.

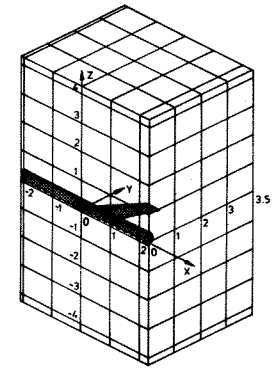

Figure 2. WING BODY CONFIGURATION IN THE COMPUTATION DOMAIN

INVESTIGATED MODELS

Three models were investigated. They all had the same wing planform, a 35° swept quarter chord line, an aspect ratio of 4, and a taper ratio of 0.4.

The PT7 model consisted of a cylindrical body with a pointed nose and a low mounted wing designed with the transonic flow program operating in the inverse mode. In the design point, $M_\infty = 0.9$, $C_L = 0.2$, a plateau pressure distribution was selected for the upper surface with a plateau Mach number of 1.3 and a linear compression towards the trailing edge. The lower surface was a compromise to obtain acceptable pressures, adequate wing thickness and a closed trailing edge. Figure 3 contains some data for the model. The wing is highly twisted and has a considerable thickness.

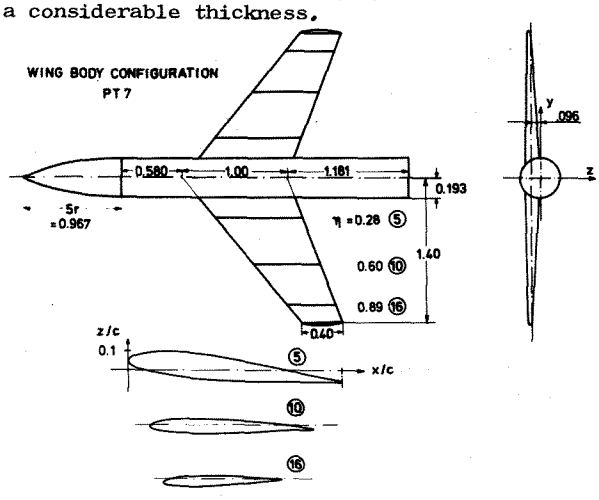

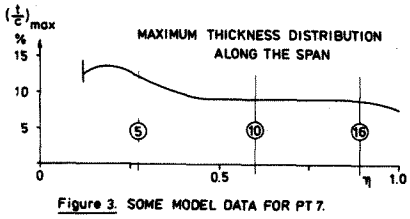

Figure 3. SOME MODEL DATA FOR PT 7.

The PT9 model differed from PT7 only in the inboard portion of the wing $\eta < 0.45$, where all vertical coordinates were reduced to obtain the thickness distribution shown in Figure 4.

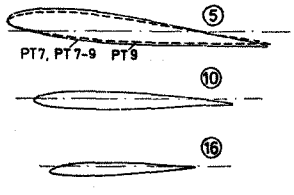

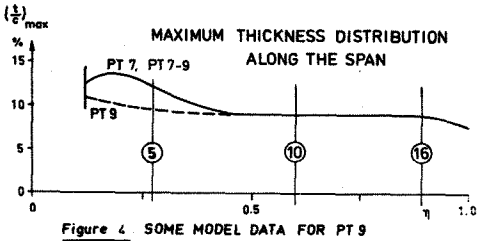

Figure 4 SOME MODEL DATA FOR PT 9

Finally the PT7-9 was a model with the PT7 wing but an indented body. The longitudinal distribution of the model cross sections was the same as for PT9 configuration. The radial reduction was at most 7 %.

Calculations of pressure distributions and lift and drag coefficients were made for all three configurations. They were carried out for Mach numbers from 0.5 to 0.95 at the angles of attack of -2°, and 0° as will be reported later [6]. However, only PT7 and PT7-9 were wind tunnel tested. The test results are to be published [7]. Balance tests were performed for Mach numbers between 0.5 and 0.97, and in general at incidences in the interval -6° to +6°. Pressures were measured for Mach numbers between 0.5 and 0.95 at incidences between -3° and 1°. The models were rather small, with a root chord of 143 mm, resulting in Reynolds numbers based on the root chord length of approximately 1.5×10^6. Transition strips were applied along a line 0.07 root chords behind the leading edge.

RESULTS

PT7

All the pressure distributions shown apply to the three chordwise stations $\eta = 0.28$, 0.60, 0.89. The comparisons are made at $\alpha = -2°$, which corresponds to a lift coefficient of 0.15 approximately, close to the design value.

Figure 5 contains a comparison between measured and calculated pressure coefficients for Mach numbers, $M_\infty = 0.90$ and 0.95. The agreement in the general features is good. The results for $M_\infty = 0.87$ and 0.92 display a very similar agreement as $M_\infty = 0.90$.

As stated before the small perturbation theory cannot be used to compute the pressures in the nose region. The straight line representation for the calculated values gives the impression of a larger discrepancy in the most forward portion of the wing than is really the case. Computed points are in x/c = 0.05, 0.14, 0.23, etc. The shock position agrees well for the outboard section, but the calculated shock inboard on the upper surface tends to be aft of where the experimental pressure distribution seems to locate it. To some degree this phenomenon is probably a boundary layer effect. Pressures on the wing's lower surface seem to be more positive in calculations.

A direct interpretation of the pressure drag is conveniently done from the pressure distributions plotted against the vertical coordinate z/c, as already has been described. Two dimensional flow calculations with Jameson's method [8] gave pressure distributions in the leading edge region which confirmed that integration by straight lines is a reasonable procedure despite the small number of points. From Figure 6, where the drag loops for $M_\infty = 0.90$ and 0.95 for three sections are shown, it can be seen that drag differences between measurements and calculations will occur due to the differences in shock positions and for the outboard section at $M_\infty = 0.95$ due to the different lower surface pressures. The figure also shows that the tangential force decreases and even becomes negative towards the outer parts. Figure 7 contains normal and tan-

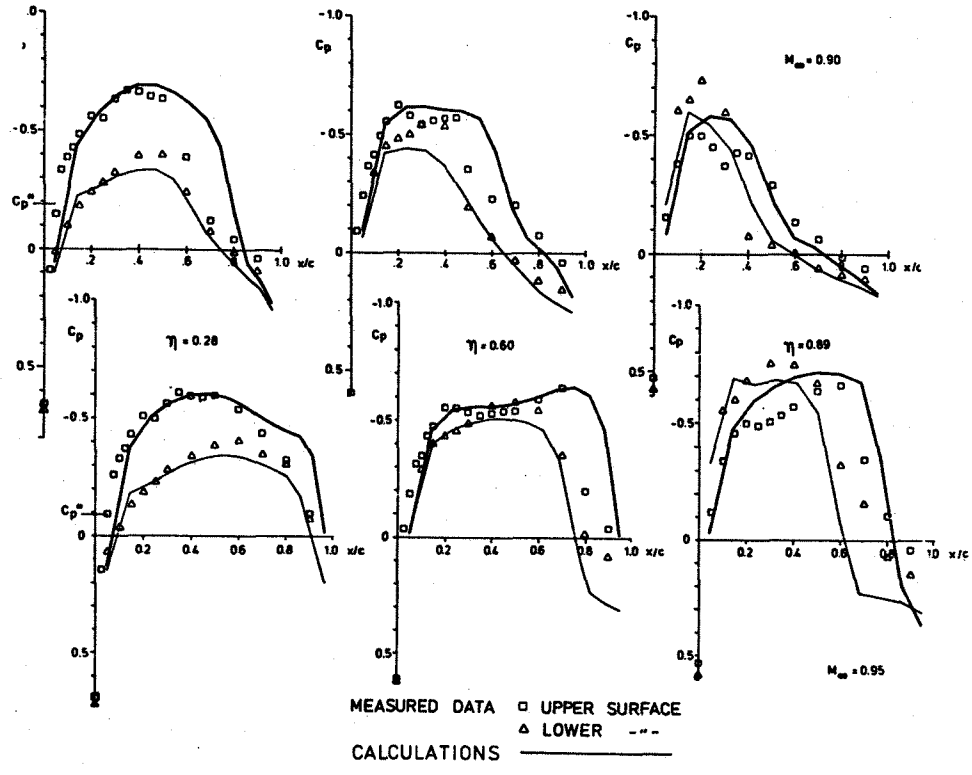

Figure 5. COMPARISON OF CALCULATED AND MEASURED PRESSURES AT $\alpha = -2^\circ$ FOR PT7

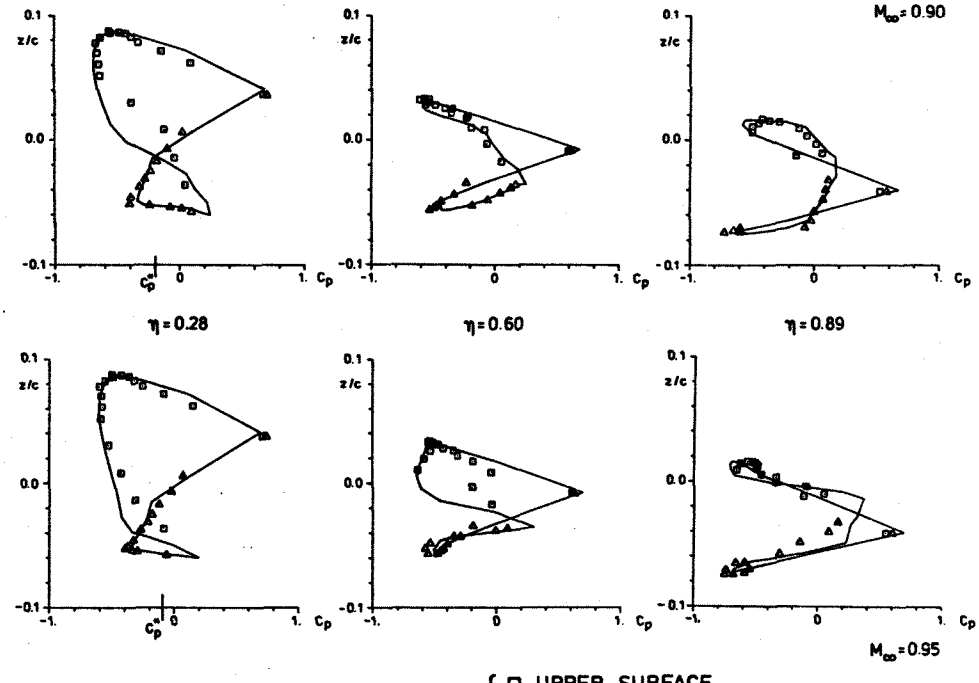

Figure 6. CALCULATED AND MEASURED PRESSURES FOR PT7 PLOTTED VERSUS z/c AT $\alpha = -2^\circ$

gential force coefficients c_n and c_t multiplied by the local chord length c to show the relevant contribution to the wing forces from each section. The distribution of drag is typical for a swept back wing, in particular for one thicker towards the root. The low outboard lift is due to the twist of the wing.

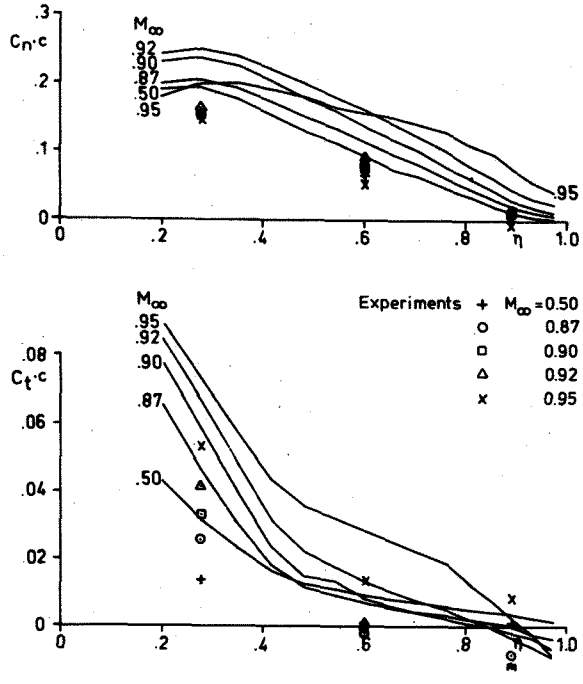

Figure 7. SPANWISE FORCE DISTRIBUTION AT α=-2° FOR PT7

The differences between measured and predicted values of c_n and c_t are partly caused by differences in shock wave positions and partly by differences in the expansion on the lower surface as could be seen in Figure 5 and Figure 6.

The calculated pressures for the wing-body combination were integrated over the wing to give lift and drag. The polars appear in Figure 8. Parabolic curves have been drawn through computed values at α= -2° and 0°, and with a vertical tangent at C_L= 0.075. The lift coefficient for minimum drag was selected from earlier extensive calculations and from analysis of the wind tunnel measurements.

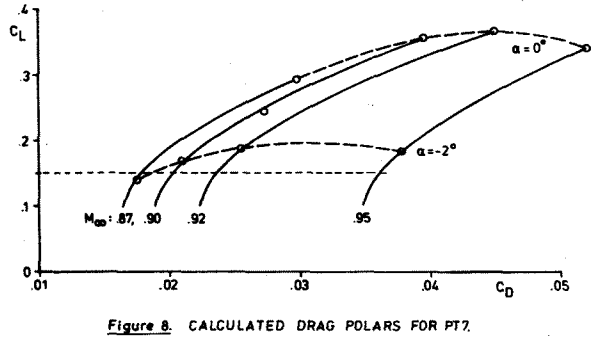

Figure 8. CALCULATED DRAG POLARS FOR PT7.

For the estimation of drag divergence Mach number the drag coefficients for a fixed lift coefficient have been extracted from the polars. To minimize the effect of curve fitting a lift coefficient of C_L = 0.15 was selected, a value that closely corresponds to α = -2°.

The cross plotted drag values appear in Figure 9. Also shown are balance measured forces with an estimated value of the nose drag subtracted. Both sets of data have been shifted to show the increments above the value for M_∞ = 0.87. A very good agreement between computed and measured data is shown. It may appear surprising because of the deviations in the pressure distributions. The explanation is probably that the total lift and drag obtained from Figure 7 yield an experimental point rather close to the calculated polar curve.

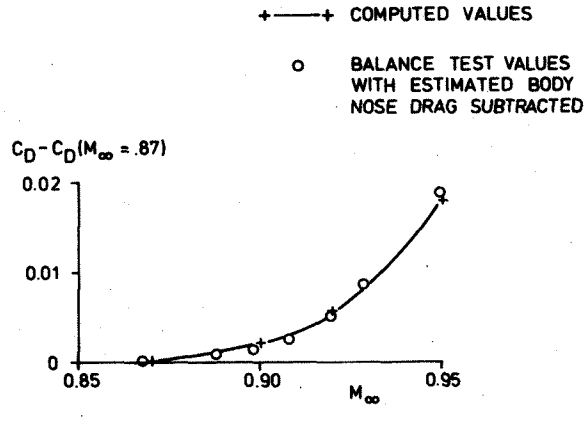

Figure 9. COMPARISON OF WING DRAG INCREMENT AT C_L= 0.15 FOR PT 7.

PT9 and PT7-9

The computed pressure distributions for all three configurations PT7, PT9 and PT7-9 at M_∞ = 0.90 and 0.95 respectively appear in Figure 10. Reduction either of inboard wing coordinates or of body cross section area mainly effect the inner portions of the wing, the influence being larger for the wing upper surface. Further out on the span both modifications give similar effects. However, on the inboard wing, η = 0.28, the influence of the contoured body is shifted downstream, because the flow is locally supersonic. The two configurations PT9 and PT7-9 have the same longitudinal distribution of cross sections but their pressure distributions differ, especially on the inboard wing.

Both experimental and theoretical values are available for PT7-9 and can be found in Figure 11.

The figure shows that the predicted reduced wing pressure level at the inboard section due to the body indentation is found also in the experiments.

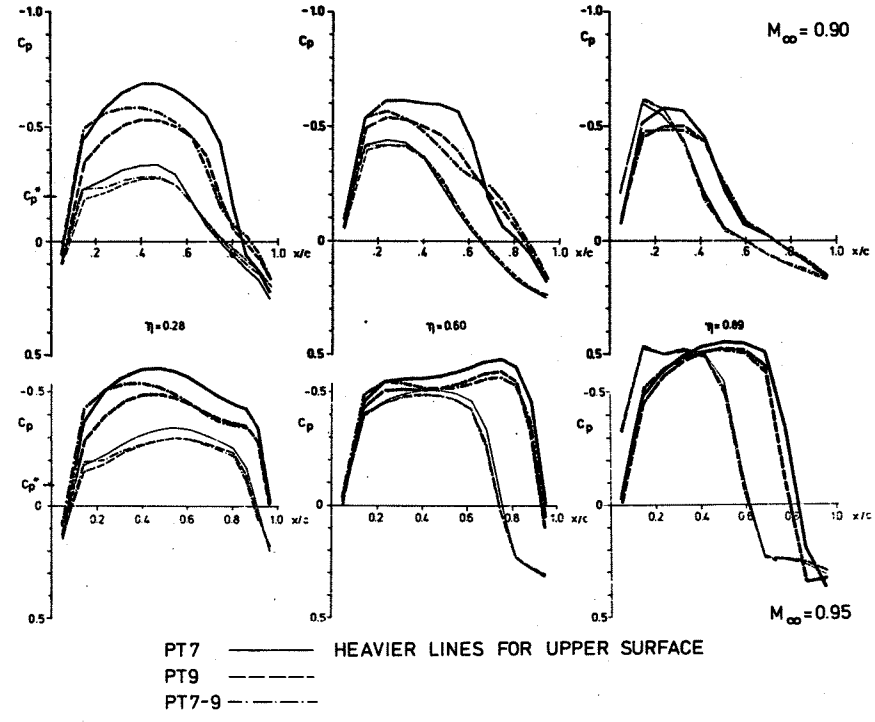

Figure 10. CALCULATED PRESSURE DISTRIBUTIONS AT $\alpha=-2°$ FOR PT7, PT9, AND PT7-9

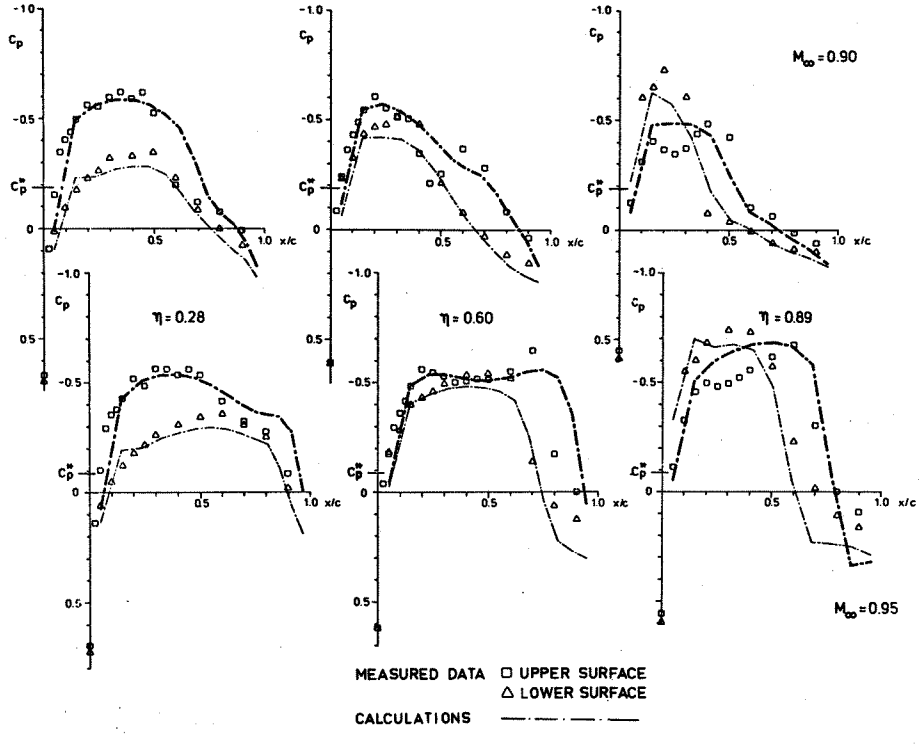

Figure 11. CAMPARISON OF CALCULATED AND MEASURED PRESSURES AT $\alpha=-2°$ FOR PT7-9

Figure 12 contains calculated pressures for all three configurations and measured values for the PT7-9, $\eta = 0.28$. PT7 and PT7-9 have a common wing and the pressure differences are due to the indented body for PT7-9. The difference results in a reduction of the positive part of the drag loop. The experiments agree well with the computations except for the shock position on the aft portion of the upper surface. Finally PT9 is a thinner wing and the drag loop is both lower and less wide.

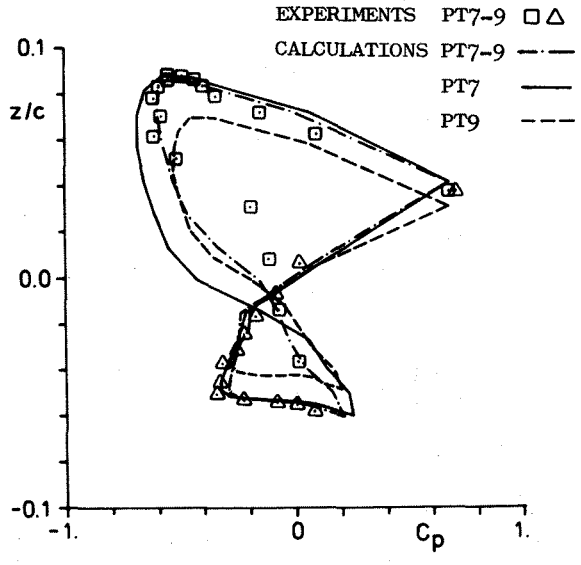

Figure 12. COMPARISON OF CALCULATED AND MEASURED PRESSURES AT $\eta = 0.28$, $\alpha = -2^{\circ}$, $M_{\infty} = 0.9$

In Figure 13 the calculated spanwise normal and tangential force distributions for the three configurations are shown for $M_{\infty} = 0.90$ and 0.95 at $\alpha = -2^{\circ}$. It is clear that especially for the tangential force distribution the main effect is at the inboard part where the geometrical modifications were made. At these rather high free stream Mach numbers one would have expected the effect of local geometrical changes to be felt all over the span, as sometimes is the case, for instance as described in reference [9]. For this wing, however, the changes in the pressure distributions which to some extent undoubtedly occur, see Figure 10, do not influence the tangential forces much.

Integration of the calculated pressures gives lift and drag from which polars have been constructed in the same way as for PT7. These polars are shown in Figure 14.

The calculated drag curve for $C_L = 0.15$ is shown in Figure 15 PT7-9 compared with the balance measurements. That the agreement for the drag rise is so good must of course, as explained earlier, be fortuitous. For comparison the calculated results for PT7 and PT9 are included. The drag of the two configurations, with the same area, distribution, PT7-9 with the indented body, and PT9 with the reduced inboard wing coordinates, are in good agreement around the

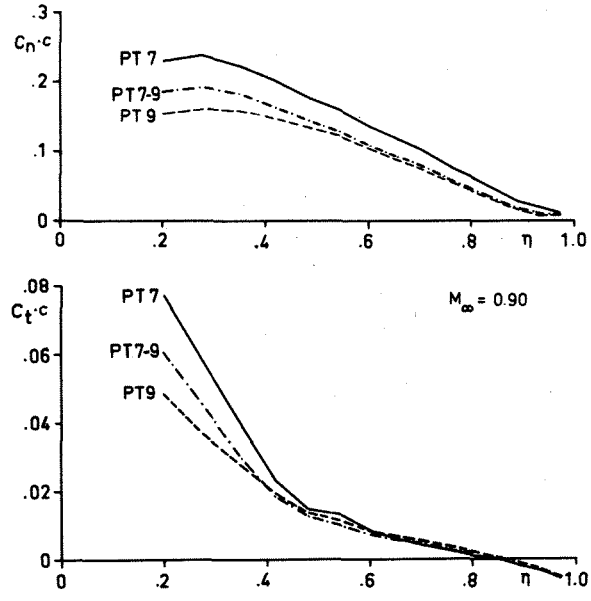

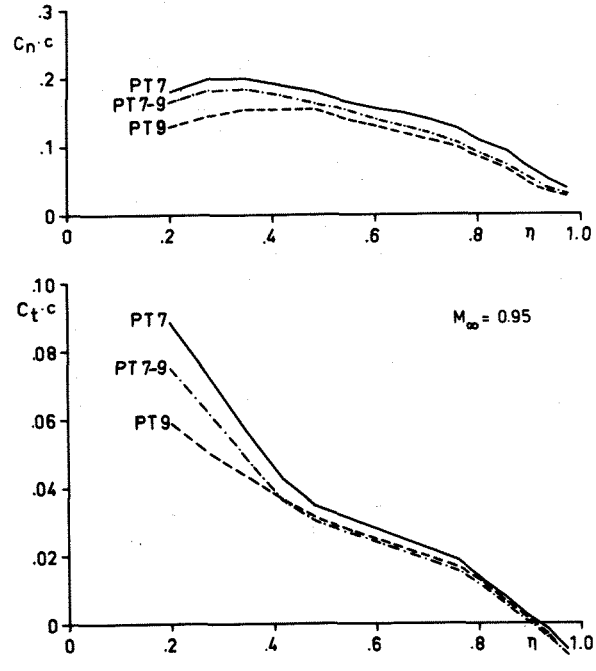

Figure 13. SPANWISE FORCE DISTRIBUTION AT $\alpha = -2$ FOR PT7, PT9 AND PT7-9

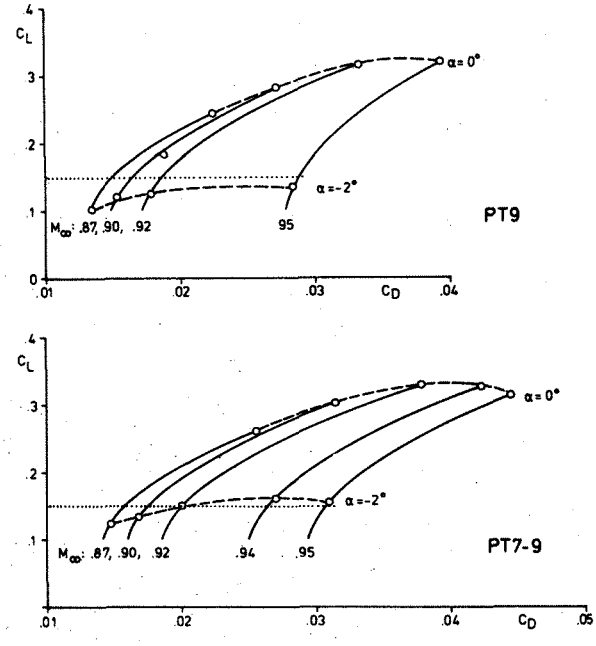

Figure 14. CALCULATED DRAG POLARS FOR PT9 AND PT7-9.

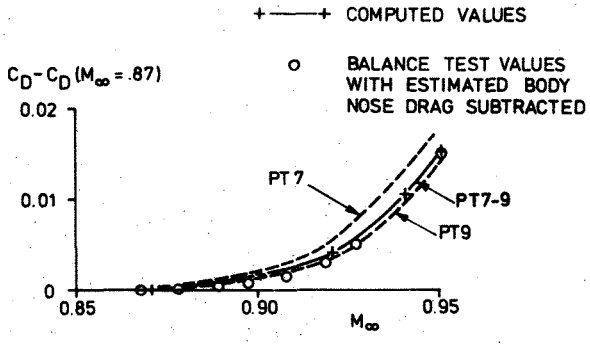

Figure 15. COMPARISON OF WING DRAG INCREMENTS FOR PT7-9 AT C_L=0.15.

lower Mach numbers ($M_\infty \approx 0.90$) but the two drag curves deviate somewhat as the Mach number is increased. The expected beneficial effect in drag rise characteristics as compared with the original wing PT7 is however verified.

CONCLUSIONS

- A calculation method based on the transonic small perturbation theory can be used in an inverse mode for the design of a wing-body combination.
- The design pressure distributions were reasonably well verified in wind tunnel tests.
- The method can be used in the direct mode for calculations outside of the design point to give transonic drag rise characteristics of the configuration.

REFERENCES

1. Schmidt, W.
Hedman, S.G.
Recent Explorations in Relaxation Methods for Three-Dimensional Transonic Potential Flow.
ICAS Paper 76-22, 1976.

2. Agrell, N.
Mattsson, R.
Nyberg, S.-E.
Investigation of the Transonic Drag Characteristics for Non-Slender Wing-Body Combinations and Their Equivalent Axisymmetric Bodies at Zero Lift.
ICAS Paper to be presented at 11th ICAS Congress, Lisbon, Portugal, Sept. 1978.

3. Murman, E.M.
Cole, J.D.
Calculation of Plane Steady Transonic Flows.
AIAA Journal, Vol. 9, No. 1, 1971.

4. Schmidt, W.
Fritz, W.
Leicher, S.
On the Proper Modelling of Three-Dimensional Transonic Flow Fields Around Supercritical Airplanes.
DGLR Paper 78-061, 1978.

5. Steger, J.L.
Baldwin, B.S.
Shock Waves and Drag in the Numerical Calculation of Isentropic Transonic Flow.
NASA TN D-6997, 1972.

6. Drougge, G.
Agrell, N.
Hedman, S.
A Comprehensive Evaluation and Analysis of Transonic Flow Calculations on Three Related Wing-Body Configurations.
FFA Technical Note AU-1418 (to appear).

7. Torngren, L.
Transonic Wind Tunnel Tests of a Swept Wing Model Designed for a Prescribed Supercritical Roof Top Pressure Distribution.
FFA Technical Note AU-1288 (to appear).

8. Jameson, A.
Numerical Computation of Transonic Flows with Shock Waves.
IUTAM, Symposium Transonicum II, Göttingen 1975, pp. 384. Springer Verlag 1976.

9. Chen, A.
Tinoco, E.
Yoshihara, H.
Transonic Computational Design Modifications of the F-111 TACT.
AIAA 16th Aerospace Sciences Meeting, Huntsville, Alabama, USA, Jan 16-18, 1978.
Paper 78-106.

ACKNOWLEDGEMENTS

This investigation has been financed by the Air Materiel Department of the Swedish Defence Materiel Administration under Contract AU-1418.